Published in final edited form as:
Nat Chem Biol. 2016 January ; 12(1): 22–28. doi:10.1038/nchembio.1965.

CRISPR-Cas9-based target validation for p53-reactivating model compounds

Michael Wanzel[1,2], **Jonas B Vischedyk**[1], **Miriam P Gittler**[1], **Niklas Gremke**[1], **Julia R Seiz**[1], **Mirjam Hefter**[1], **Magdalena Noack**[1], **Rajkumar Savai**[2,3,4], **Marco Mernberger**[1], **Joël P Charles**[1], **Jean Schneikert**[1], **Anne Catherine Bretz**[1], **Andrea Nist**[1,5], and **Thorsten Stiewe**[1,2,5,*]

[1]Institute of Molecular Oncology, Philipps University, Marburg, Germany

[2]Universities of Giessen and Marburg Lung Center (UGMLC), German Center for Lung Research (DZL), Germany

[3]Max Planck Institute for Heart and Lung Research, Department of Lung Development and Remodeling, Bad Nauheim, Germany

[4]Department of Internal Medicine, Justus Liebig University, Giessen, Germany

[5]Genomics Core Facility, Philipps University, Marburg, Germany

Abstract

Inactivation of the p53 tumor suppressor by Mdm2 is one of the most frequent events in cancer, so compounds targeting the p53-Mdm2 interaction are promising for cancer therapy. Mechanisms conferring resistance to p53-reactivating compounds are largely unknown. Here we show using CRISPR-Cas9–based target validation in lung and colorectal cancer that the activity of nutlin, which blocks the p53-binding pocket of Mdm2, strictly depends on functional p53. In contrast, sensitivity to the drug RITA, which binds the Mdm2-interacting N terminus of p53, correlates with induction of DNA damage. Cells with primary or acquired RITA resistance display cross-resistance to DNA crosslinking compounds such as cisplatin and show increased DNA cross-link repair. Inhibition of FancD2 by RNA interference or pharmacological mTOR inhibitors restores RITA sensitivity. The therapeutic response to p53-reactivating compounds is therefore limited by compound-specific resistance mechanisms that can be resolved by CRISPR-Cas9-based target validation and should be considered when allocating patients to p53-reactivating treatments.

*Correspondence and requests for materials should be addressed to T.S. thorsten.stiewe@uni-marburg.de.

Author contributions

M.W., J.B.V., M.P.G., N.G., M.H., M.N., J.P.C., J.R.S., J.S. and A.C.B. designed, performed and analyzed experiments. A.N. performed next-generation sequencing. M.M. performed bioinformatic data analysis. R.S. provided critical reagents. M.W. and T.S. wrote the manuscript with advice from all authors. M.W. and T.S. guided all aspects of this study.

Competing financial interests

The authors declare no competing financial interests.

Additional information

Reprints and permissions information is available online at http://www.nature.com/reprints/index.html.

Europe PMC Funders Author Manuscripts

Cancer development is driven by the combined activation of oncogenic signaling and the inactivation of tumor suppressive pathways. Although chemical inhibitors of oncogenic signaling have entered current clinical practice, the complementary and technically more challenging approach of reactivating tumor suppressors is still in the beginning stages. The most commonly inactivated tumor suppressor is p53, and genetic mouse models have provided proof-of-concept evidence that tumors become addicted to p53 inactivation and respond to p53 restoration with tumor regression1–5. Approximately half of all cancer patients have a mutated *TP53* gene, which encodes p53 (refs. 1–6). In the remainder of patients with a wild-type *TP53* gene, p53's activity is inhibited, for example, by the E3 ubiquitin ligase Mdm2, which binds it, inhibits its transcriptional activity and targets it for proteasomal degradation1,7. Compounds that interfere with the p53-Mdm2 interaction, release p53 from inhibition and thereby reactivate its tumor suppressor activity are considered promising for a broad spectrum of cancer therapies7.

X-ray crystallography revealed that Mdm2 has a deep hydrophobic cleft on which p53 binds with its N-terminal domain and provided the basis for the identification of nutlin as what is to our knowledge the first chemical compound to reactivate p53 by occupying the p53-binding pocket on Mdm2 (refs. 8,9). Here, crystal structures of Mdm2 in complex with nutlin-3a, the active isomer of nutlin, guided the design of better nutlin-type inhibitors, some of which are currently being tested in ongoing clinical trials10. Underscoring the role of nutlin's on-target activity for tumor therapy, cancer cell lines adapted to nutlin exhibit a high frequency of p53 gene mutations, unlike the majority of cells with acquired resistance to classical genotoxic compounds11. The correlation between nutlin sensitivity and p53 mutations was consistently the most significant ($P < 1 \times 10^{-36}$) drug-gene association identified in a large high-throughput screen comprising 639 human tumor cell lines and 130 drugs12. Nevertheless, there is also evidence for p53-independent effects of nutlin: for example, nutlin releases the p53 family member p73 and E2F1 from inhibition by Mdm2 and reverses MDR1- and MRP1-induced drug resistance in an Mdm2-independent manner13,14.

In addition, cell-based screens for activators of the p53 pathway were instrumental in identifying further inhibitors of the p53-Mdm2 interface. For example, 2,5-bis(5-hydroxymethyl-2-thienyl) furan (NSC652287), a known genotoxic compound15, was found to specifically kill parental (wild-type p53) HCT116 colorectal cancer cells but not a derivative subclone in which the p53 gene had been disrupted by homologous recombination16,17. This thiophene compound was therefore designated RITA for 'reactivation of p53 and induction of tumor cell apoptosis'16. In contrast to nutlin-type compounds, RITA was found to disrupt the p53-Mdm2 interaction by binding the N terminus of p53 (ref. 16). Thus, nutlin and RITA both interfere with the p53-Mdm2 interaction: one binds Mdm2, and the other binds p53. However, they affect cells in a remarkably different manner. Although nutlin induces cell cycle arrest in the majority of wild-type p53 cells18,19, RITA induces a strong apoptotic response16. This is in part explained by nutlin binding to Mdm2 and inhibiting Mdm2-dependent degradation of hnRNP K, a p53 cofactor required for p21-dependent G1 cell cycle arrest19. Thus, high levels of hnRNP K in cells treated with nutlin, but not RITA, favor p21-mediated cell cycle inhibition and protect nutlin-treated cells from killing19. Furthermore, the apoptotic

response induced by RITA is dose dependent and is accompanied by transcriptional repression of anti-apoptotic proteins and ROS defense pathways, blocking of the Akt pathway and downregulation of key oncogenic signaling pathways20,21. In light of the proposed mode of action described above, it was rather unexpected that RITA was later also found to reactivate mutated p53 proteins, possibly by triggering a conformational change propagating from the N terminus to the rest of the protein, which promotes proper folding of mutant p53 (refs. 22–24).

A key problem in the clinical application of molecularly targeted drugs is the rapid development of drug resistance. Identification of the underlying mechanisms, however, is not only essential for overcoming resistance but also for predicting drug sensitivity, selecting suitable patients for clinical trials and for eventually allocating patients to the most promising treatment. As a common characteristic of p53-Mdm2 interaction inhibitors is that they reactivate the tumor suppressor function of p53, it would be expected that their activity is dependent on p53. However, chemical compounds are often less specific than antibodies and RNA interference, resulting in off-target activities. These not only cause adverse side effects but also contribute to the therapeutic activity in a poorly understood manner that differs between individual compounds25. In recent years, advances in genome editing with the CRISPR-Cas9 system have proven to be powerful for validating genes as drug targets26–28. For example, cells with CRISPR-Cas9–induced indel mutations in the *HPRT1* gene were shown to be enriched from heterogeneous cell mixtures by the antimetabolite 6-thioguanine (6-TG), confirming the importance of HPRT1 for 6-TG–induced cell death26.

We therefore used CRISPR-Cas9–mediated gene editing to explore the extent to which the anti-tumor activities of nutlin and RITA as p53-reactivating model compounds depend on the presence of functional wild-type p53. Though we confirm that nutlin inhibits tumor cell proliferation in a p53-dependent manner, we find p53 to be entirely dispensable for the activity of RITA. Instead, we show that RITA functions as a genotoxic compound that induces DNA damage so that its therapeutic efficacy becomes limited by DNA repair. In particular, we identify the mTOR-regulated Fanconi anemia pathway as responsible for primary and acquired resistance to RITA. Together these data indicate that RITA's mode of action is not p53 dependent but DNA damage dependent, thus highlighting the power of the CRISPR-Cas9 system to explore and dissect modes of drug action.

Results

RITA is active without p53

Nutlin and RITA were both initially identified as compounds that exhibit antiproliferative activity in wild-type p53 tumor cells but not in p53-mutated or p53-deleted cells9,16. In particular, RITA was identified in a cell-based screen for compounds with activity in wild-type p53 HCT116 cells but not in an HCT116 subclone engineered to be p53 deficient by homologous recombination16,17. In light of accumulating reports that RITA is also effective in various p53-mutated cell lines22–24, we aimed to explore the p53 dependence of the two p53-reactivating model compounds more systematically using CRISPR-Cas9-mediated gene disruption. p53-proficient HCT116 colorectal and H460 lung cancer cells that respond well to both nutlin (half-maximum inhibitory concentration (IC_{50}): 5 μM) and RITA (IC_{50}: 0.25

μM) were transfected with Cas9 and several subgenomic single guide RNAs (sgRNAs) previously validated to successfully target different coding regions of *TP53* (Fig. 1a,b). Consistent with data showing that Cas9-induced double-strand breaks are repaired most commonly by error-prone nonhomologous end joining, deep sequencing of PCR amplicons spanning the nuclease target sites detected various indel mutations (Fig. 1C). By keeping the transfection efficiency low, we detected indels in a low percentage (<4%) of cells. The percentage of indels progressively increased to 70–90% after 17 d of treatment with nutlin, whereas no enrichment was observed in untreated cultures (Fig. 1C). In marked contrast to the effect of nutlin, enrichment of indels was not consistently observed in the presence of RITA. The sequencing results were confirmed by semiquantitative assessment of indels with T7 endonuclease assays (Supplementary Results, Supplementary Fig. 1).

As CRISPR-Cas9–induced indels can give rise to production of truncated proteins or mutated proteins with subtle amino acid deletions or insertions, we also generated *p53* gene deletions spanning most of the coding sequence using two pairs of sgRNAs targeting *TP53* introns 1 and 9 (Fig. 1b). Using primer pairs flanking the expected breakpoint region, we observed strong enrichment of deleted alleles in the presence of nutlin but not RITA (Fig. 1d). Likewise, a competitive cell culture assay confirmed enrichment of HCT116 depleted of p53 by RNA interference (RNAi) in the presence of nutlin but not RITA (Supplementary Fig. 2)29. Together, these findings indicate that *TP53* mutations, *TP53* gene deletions and p53 knockdown confer a selective growth advantage under competitive culture conditions in the presence of nutlin but not RITA. This suggests that only the antiproliferative activity of nutlin is strictly dependent on the presence of functional p53.

To further substantiate these observations, we generated various p53-deficient HCT116 and H460 single-cell clones and tested their response to either nutlin or RITA in clonogenic survival assays (Fig. 1e and Supplementary Fig. 3). Although the previously reported p53-deficient HCT116 *TP53*$^{-/-}$ cells17 were indeed refractory to both nutlin and RITA, the vast majority of p53-deficient cell clones with CRISPR-Cas9–generated small indels or large gene deletions were only resistant to nutlin. Using western blotting and Sanger sequencing, we confirmed the absence of wild-type p53 in these clones (Fig. 1e and Supplementary Fig. 3). A control clone, targeted with a GFP-directed Cas9 nuclease, retained sensitivity to both nutlin and RITA. Notably, the sensitivity of p53-null clones to RITA cannot be explained by the off-target effects of the used sgRNAs as p53-deficient clones generated with multiple different sgRNA sequences showed similar results. We therefore conclude that nutlin but not RITA requires functional p53 to inhibit tumor cell proliferation.

RITA sensitivity correlates with induction of DNA damage

Remarkably, a few p53-deficient HCT116 and H460 clones showed resistance to both nutlin and RITA similar to the original HCT116 *TP53*$^{-/-}$ clone17 (Fig. 1e and Supplementary Fig. 3), hinting at p53-independent mechanisms of RITA resistance that can be acquired or selected under treatment. In line with this hypothesis, H460 cells and various other RITA-sensitive cell lines spontaneously gave rise to RITA-resistant clones when continuously cultured in the presence of RITA for a few weeks (Supplementary Fig. 4a-c). We did not observe cross-resistance to nutlin, indicating that functional p53 was retained

(Supplementary Fig. 4b,c). Furthermore, although A549 cells carry wild-type p53 and are sensitive to nutlin, they show primary resistance to RITA (Supplementary Fig. 4c). RITA resistance is therefore independent of p53 status and caused by other mechanisms.

Notably, RITA resistance of H460-derived subclones was reversible and lost upon continuous long-term culturing in the absence of RITA, suggesting a nongenetic cause of resistance (Supplementary Fig. 5). Furthermore, we could confirm by measuring the autofluorescence of RITA that resistant clones do not show defects in RITA internalization or enhanced RITA export (Supplementary Fig. 6). Pharmacological or RNAi-mediated inhibition of ATP binding-cassette transporters consistently did not resensitize resistant cells (Supplementary Figs. 7 and 8). All of the wild-type p53 cell lines that became RITA resistant responded to nutlin treatment by accumulating p53 and upregulating the p53 target gene encoding the cyclin-dependent kinase inhibitor $p21^{CDKN1A}$, thus excluding a defect in the antiproliferative p53 downstream signaling pathways (Fig. 2a,b). However, RITA did not stabilize p53 in the resistant subclones and failed to activate $p21^{CDKN1A}$, suggesting a defect in the upstream regulation of p53.

As previous reports have suggested that RITA induces DNA damage and that p53 is engaged by DNA damage signaling22,30, we analyzed our panel of RITA-sensitive and resistant cell clones for markers of DNA damage, which yielded a marked correlation between RITA sensitivity and induction of H2A.X phosphorylation as a common marker for double-strand breaks (Fig. 2c,d and Supplementary Fig. 9). All of the RITA-sensitive cell lines showed massive accumulation of γH2A.X, whereas the original HCT116 $TP53^{-/-}$ cells; primary resistant A549 cells; and our few CRISPR-generated, p53-null RITA-resistant clones did not. We concluded that RITA resistance is not mediated by p53 mutations but rather by defects in DNA damage signaling, which is known to engage both p53-dependent and p53-independent arms. Thus, the absence of RITA resistance upon p53 inactivation is explained.

RITA resistant cells are cross-resistant to cisplatin

Given that RITA resistance is correlated with a reduced ability to induce DNA damage signaling, we tested for cross-resistance to DNA-damaging compounds in clinical use. RITA-resistant H460 cells showed marked cross-resistance to various DNA cross-linkers including cisplatin (CDDP), oxaliplatin, carmustin and mitomycin C but not to chemotherapeutics such as hydroxyurea or the nucleoside analog cytarabin (AraC) (Fig. 3a). Conversely, cells adapted to cisplatin by dose escalation exhibited cross-resistance to RITA, but not nutlin (Fig. 3b). Furthermore, parental and RITA- and CDDP-adapted H460 cells showed comparable signs of DNA damage, as measured by γH2A.X induction as early as 6 h after a 2-h treatment with CDDP (Supplementary Fig. 10). Although DNA damage further progressed in parental cells 46 h after discontinuation of CDDP, the γH2A.X signal largely disappeared in both RITA- and CDDP-resistant cells, consistent with an enhanced ability for DNA repair (Fig. 3C). Notably, RITA was shown to act as a DNA cross-linking agent before it was described to target the p53-Mdm2 interaction15,16, thus providing an explanation for cross-resistance. Our results suggest that the genotoxic activity of RITA dominates possible direct effects on p53 and that DNA repair properties determine the resistance profile for this compound.

RITA resistance is mediated by FancD2

The most toxic lesion resulting from cisplatin-DNA adducts are DNA interstrand crosslinks (ICLs) that progress to deleterious double-strand breaks upon DNA replication31. Cisplatin resistance is often acquired because of increased ICL repair32, a process that requires the Fanconi anemia (FA) pathway to coordinate three critical DNA repair processes, including nucleolytic incision, translesion DNA synthesis and homologous recombination33. Central to this pathway is FancD2, which coordinates the multiple DNA repair activities required for the resolution of crosslinks33. We therefore explored whether FancD2 is responsible for RITA resistance. Consistent with our hypothesis, transient or stable knockdown of FancD2 effectively resensitized various different RITA-resistant cell types not only to cisplatin and oxaliplatin but also to RITA (Fig. 4 and Supplementary Figs. 11-13). First, stable FancD2 knockdown cells were progressively depleted from cocultures in the presence of RITA (Fig. 4a and Supplementary Fig. 11). Second, transient FancD2 knockdown resensitized parental and RITA-adapted H460 and U2OS cells to RITA, cisplatin and oxaliplatin, resulting in reduced clonogenic growth (Fig. 4b and Supplementary Fig. 12a). We observed restoration of sensitivity to RITA not only in cells that were experimentally rendered resistant by long-term adaptation to RITA but also in various lung cancer cells with primary RITA resistance (Supplementary Fig. 12b-d). Notably, FancD2 depletion overcame resistance irrespective of p53 status. Depletion of FancD2 also rendered the original HCT116 *TP53*$^{-/-}$ cell clone17 highly sensitive to RITA, indicating that its reported RITA resistance is not due to its p53 deficiency but rather caused by increased FancD2-mediated DNA repair (Fig. 4c,d). Likewise, FancD2 depletion also resensitized the single p53-deficient, RITA-resistant HCT116 clone i5#2 (Supplementary Fig. 13). Notably, we observed no resensitization upon depletion of FancA and FancL, which are essential components of the FA core complex that functions as a multisubunit E3 ubiquitin ligase complex for the regulatory monoubiquitination of FancD2 (Supplementary Fig. 14). This is consistent with the notion that the FA pathway is not linear and that several protein subcomplexes with different functions exist34. Instead, sensitivity was restored upon Rad18 depletion, which has been reported as an alternative E3 ubiquitin ligase for FancD2 (Fig. 5a and Supplementary Fig. 15)35–39. In fact, both Rad18 and FancD2 proteins were found to be frequently upregulated in RITA and cisplatin-resistant cell lines (Fig. 5b and Supplementary Fig. 16).

Consistent with FancD2's role in resolving RITA-induced DNA crosslinks and preventing the progression of stalled replication forks via RPA32^{pS33}-positive single-strand breaks to γH2A.X-labeled double-strand breaks, FancD2 depletion restored the ability of RITA to induce RPA32^{pS33} and H2A.X phosphorylation in resistant cell clones (Fig. 5C).

RITA resistance is overcome with mTOR inhibitors

FancD2 has been shown to be regulated by mTOR signaling, offering a perspective for targeting resistance to RITA and other DNA crosslinking compounds with pharmacological mTOR inhibitors40,41. FancD2 upregulation in RITA-resistant cells was indeed accompanied with elevated mTOR signaling activity, as shown by increased phosphorylation of 4EBP1 and p70S6K (Fig. 6a). mTOR kinase inhibition with AZD8055 reversibly reduced FancD2 expression in a time-dependent manner (Fig. 6b,c) and sensitized both parental and RITA-resistant H460 cells to RITA treatment (Fig. 6d). Consistent with a specific effect of

AZD8055-mediated downregulation of FancD2 on DNA repair, AZD8055 restored the ability of RITA to induce γH2A.X in resistant cells (Fig. 6e). Furthermore, AZD8055 also sensitized RITA-resistant cells to cisplatin and cisplatin-adapted cells to RITA (Fig. 6f). Confirming the target specificity of AZD8055, RNAi-mediated depletion of mTOR likewise sensitized cells to RITA and cisplatin treatment (Fig. 6g,h).

We conclude that RITA resistance occurs independently of p53 through mTOR-mediated upregulation of FancD2-dependent DNA cross-link repair, whereas mTOR inhibition downregulates FancD2 and prevents repair of RITA-induced DNA cross-links, thereby effectively counteracting RITA resistance.

Discussion

Mdm2 is a key inhibitor of p53 that targets wild-type p53 for degradation and allows tumor cells to evolve in the absence of p53 gene mutations. Targeting the interaction between Mdm2 and p53 is therefore a very promising therapeutic strategy as reactivation of the p53 tumor suppressor could nicely complement the clinically practiced inhibition of oncogenic signaling pathways7,10. A protein-protein interaction can be blocked in a straightforward manner by targeting compounds to the interaction interface on either one of the two interacting proteins. Although nutlin was designed to fit into the p53-binding groove on Mdm2, RITA was shown to bind to p53. In principle, both strategies should result in similar outcomes, depend on identical effectors and be limited by the same resistance mechanisms. It was therefore rather surprising to see that the inhibitory effect of nutlin on tumor cell proliferation strictly relied on the presence of wild-type p53, whereas the activity of RITA did not. Multiple RITA-sensitive cell lines retained RITA responsiveness upon disruption of the p53 ORF by indel-induced frameshift mutations, p53 gene deletion with paired CRISPR-Cas9 nucleases or p53 mRNA downregulation by RNAi. In contrast, the response to nutlin was lost in all cases. These experiments performed in several cell lines with independent methods conclusively demonstrate that the two p53-Mdm2 interaction inhibitors nutlin and RITA differentially depend on wild-type p53.

In line with our observation of p53-independent RITA activity, RITA has recently been reported to kill not only p53 wild-type cells but also cells expressing mutant p53 (refs. 22–24). It was hypothesized that binding of p53 to the N terminus of the mutant p53 protein could drive p53 folding into a wild type–like, active conformation23. Alternatively, RITA might not be a direct inhibitor of the p53-Mdm2 interaction but rather disrupt the interaction indirectly by triggering DNA damage signaling–dependent, ATM/CHK2-mediated phosphorylation of p53, similar to other genotoxic compounds. In line with this, NMR studies failed to demonstrate RITA-induced disruption of a p53–Mdm2 complex *in vitro*42. Likewise, RITA but not nutlin triggers extensive phosphorylation at the DNA damage–responsive p53 residue Ser15, and CHK2-deficient HCT116 cells are refractory to RITA but not nutlin30.

We now show in this study that RITA activity directly correlates with the ability to induce DNA damage, as measured by H2A.X phosphorylation of Ser139. Furthermore, RITA resistance is associated with remarkable cross-resistance to various DNA cross-linking

drugs, including cisplatin. As resolution of DNA ICLs requires the concerted action of multiple DNA repair pathways, we tested the role of FancD2, a central coordinator of ICL repair33, in RITA resistance. In all instances of primary or acquired RITA resistance, RITA sensitivity was restored upon knockdown of FancD2 or inhibition of mTOR, an upstream regulator of FancD2 expression40,41. Furthermore, FancD2-depleted or mTOR-inhibited cells failed to acquire RITA resistance under long-term treatment. Most notably, the original HCT116 *TP53*$^{-/-}$ cell line17, which was instrumental in the identification of RITA as a p53-reactivating compound16, was rendered RITA sensitive by FancD2 depletion, proving that the resistance of HCT116 *TP53*$^{-/-}$ cells is not due to their p53 deficiency.

When RITA-sensitive cells were cultured in long-term clonogenic assays, they consistently gave rise to multiple RITA-resistant subclones. This behavior is reminiscent of cancer stem cells, which express high levels of ABC transporters that confer drug resistance43,44. However, pharmacological or RNAi-mediated inhibition of ABC transporters did not overcome the resistance to RITA (Supplementary Figs. 7 and 8). Notably, A549 cells that express wild-type p53 but are nevertheless intrinsically resistant to RITA exhibit an exceptionally high fraction of cancer-initiating cells45,46. Together, these data suggest that the RITA-resistant phenotype is present or develops in the cancer stem cell fraction but can be maintained independent of stemness.

In summary, our study identified remarkably different resistance mechanisms to two model p53-reactivating compounds that were described to target the p53-Mdm2 interaction from two different sides. Using CRISPR-Cas9 genome engineering to introduce small indel mutations and long deletions into the p53 gene, we confirm a strictly p53-dependent anti-proliferative activity of nutlin. In parallel, the results question direct targeting of the p53-Mdm2 interaction by RITA and instead suggest that RITA primarily acts as a cross-linking drug whose activity is limited by mTOR-FancD2–mediated DNA repair. CRISPR-Cas9 genome editing was therefore extremely powerful in dissecting the mode of action of p53-reactivating compounds. As different modes of action are limited by distinct resistance mechanisms, such studies should be implemented extensively before clinical trials are initiated to identify groups of cancer patients whose genetic profile most likely predicts a therapeutic benefit from the tested compound.

Online Methods

Cell culture

All cell lines were obtained from the American Tissue Collection Center (ATCC) and grown in high-glucose Dulbecco's Modified Eagle’s Medium (HCT116, A549, U2OS) or Roswell Park Memorial Institute Medium 1640 medium (H460, H661) supplemented with 10% FBS, 100 U ml^{-1} penicillin and 100 μg ml^{-1} streptomycin at 37 °C with 5% CO_2. p53-deficient HCT116 *p53*$^{-/-}$ cells were generously provided by B. Vogelstein (Johns Hopkins University)17. Cell lines were regularly tested by PCR for mycoplasma contamination and used for less than 25 passages after revitalization. Transduced cell lines were maintained in 1 μg ml^{-1} puromycin. For induction of doxycycline-regulated vectors, cell culture medium was supplemented with 1–2 μg ml^{-1} doxycycline (Sigma). Cells were treated with 1–2 μM RITA (Merck) and 5–10 μM nutlin-3a (Merck). Chemical structures of all compounds are

shown in Supplementary Figure 17. CDDP was used at 3 μM, oxaliplatin at 8 μg ml^{-1}, carmustin at 50 μg ml^{-1}, mitomycin C (MMC) at 0.05 μg ml^{-1}, cytarabin (AraC) at 0.5 μg ml^{-1} and hydroxyurea at 0.5 mM. AZD8055 (ref. 47) (Selleckchem) was used at a concentration of 1–2 μM.

RITA-resistant cells were generated by continuous treatment with 1 μM RITA or by dose escalation from 0.005 μM to 2.56 μM RITA. CDDP-resistant cells were generated with CDDP in the same concentration range for dose escalation or by constant treatment with 2 μM CDDP. Resistant cells were maintained with 1 μM CDDP or 1 μM RITA, respectively. Cell titer was measured using the CellTiter-Glo reagent from Promega according to the manufacturer's instructions. For colony formation assays, cells were plated 1 d before treatment. Cells were cultivated for further 10 d before they were fixed with 70% ethanol overnight, stained with Giemsa solution and quantified using the ImageJ plugin ColonyArea48. Luciferase assays with cell culture medium were carried out as described previously29.

Lentiviruses

293T cells were transfected with the calcium-phosphate method using lentiviral vector plasmids and packaging plasmids pMD2.G and psPAX2 (Didier Trono, Addgene plasmids 12259 and 12260). Supernatants containing lentiviruses were collected on the second and third day after transfection and concentrated by polyethylene glycol precipitation. For lentiviral transduction, cells were seeded on six-well plates and infected with concentrated lentivirus in the presence of polybrene (8 μg ml^{-1}) and spin infection (1 h, 1,500 r.p.m., 37 °C). Cells were selected with puromycin (2 μg ml^{-1}) for 5 d.

RNAi

For siRNA transfection cells were plated at a density of 50–80% on 6-cm dishes 1 d before transfection. siRNAs were purchased from Dharmacon and were used at a final concentration of 20 nM. Transfection was carried out using the Lipofectamine RNAiMAX reagent (Invitrogen) according to the manufacturer's instructions. Lentiviral vector plasmids for stable, constitutive or inducible expression of secreted luciferases GLuc and CLuc coupled to p53 or nontargeting control shRNAs were described previously29. shRNA sequences from Open Biosystems are as follows: shFancD2.2 (V2LHS_139155), shFancD2.3 (V3LHS_383034), shFancD2.4 (V3LHS_383035). siRNA sequences: siFancD2.6 CAACATACCTCGACTCATT, siFancD2.8 GGAGATTGATGGT CTACTA, simTOR.8 GGCCAUAGCUAGCCUCAUA, simTOR.9 CAAAGGA CUUCGCCCAUAA, simTOR.10:GCAGAAUUGUCAAGGGAUA, simTOR.11 CCAAAGCACUACACUACAA.

CRISPR-Cas9 and sequencing

For the generation of p53 knockout cells using CRISPR-Cas9 gene editing, sgRNAs targeting the *TP53* gene were cloned into pX330-U6-Chimeric_BB-CBh-hSpCas9 and lentiCRISPR v1 vectors (Addgene) as previously described49. sgRNA sequences are as follows: i1.1 TCTGCAGGCCCAGGTGA.CCCagg, i1.2 GGGTTGGAAGTGTCTCA.TGCtgg, e3 ACTTCCTGAAAACAACG.TTCtgg, e5.1 GGGGGTGTGGAATCAAC. CCAagg, e5.2 GTTGATTCCACACCCCC.GCCcgg, i5

GATTCCTCACTGA TTGC.TCTtag, e7 CCGGTTCATGCCGCCCA.TGCagg, i9 GAAACTTTCCA CTTGAT.AAGagg, GFP GGAGCGCACCATCTTCT.TCAagg.

For enrichment assays, HCT116 and H460 cells were transfected with pX330 vectors carrying sgRNAs targeting coding exons of *TP53*. Six days after transfection, cells were either left untreated or were treated with 7 μM nutlin-3a or 1 μM RITA for up to 10 d. After harvesting the cells, genomic DNA was isolated using the QIAamp DNA Blood Mini Kit according to the manufacturer's instruction and used for the T7 endonuclease I assay, deep sequencing and qPCR. For generating p53 knockout cell clones with small indel mutations, H460 and HCT116 were infected with lentiviral vectors (lentiCRISPR)50 coexpression Cas9 and sgRNAs targeting central *TP53* regions and selected with puromycin. For generating p53 knockout cell lines with deletions of exons 2 to 9, HCT116 cells were cotransfected with two pX330 plasmids containing sgRNAs targeting *TP53* intron 1 and intron 9. Single-cell clones were tested for the presence of the deletion and absence of wild-type sequence by PCR, expanded and used for further experiments.

For sequencing of indel mutations, the region surrounding the predicted cleavage site was amplified using barcoded primers: e3_fw ACGGCAAGGGGGACTGTAG; e3_rev AGCCCCCTAGCAGAGACCTG; e5.1_fw GTGCTGTGACTGCTTGTAGATGGC; e5.1_rev CCTGACTTTC AACTCTGTCTCCTTCCTC; e5.2_fw TCCAGCCCCAGCTGCTCAC; e5.2_ rev TTGCCAACTGGCCAAGACCT. PCR products were purified and equimolar amounts were pooled. DNA (10 ng) were processed using the NEBNext ChIP-Seq Library Prep Master Mix Set (New England BioLabs). The resulting library was sequenced on a MiSeq (Illumina). Sequencing library quality and quantity was evaluated on a Bioanalyzer DNA High Sensitivity chip (Agilent) and by digital PCR, respectively. Sequencing was performed on a MiSeq (Illumina) using a 6-pM library concentration and MiSeq v2 reagent kit and flow cell in a 2 × 250 base paired-end run. Multiplexed reads were demultiplexed into separate amplicon-specific lanes by the barcoded primer combinations using an error-tolerant primer detection method using the cutadapt algorithm (maximal error rate = 0.04). Lanes were subsequently aligned with the Bowtie2 mapper (standard parametrization) to the reference genome (Ensembl revision 77, GRCh38). Reads covering the regions of interest were extracted from the aligned lanes and insertions or deletions were directly inferred from the CIGAR strings. We reported indel percentages as the number of reads carrying an insertion or deletion divided by the total number of reads covering the putative Cas9 cleavage site. Our estimates were confirmed by using the VarScan2 variant caller. As indel detection depends on an accurate alignment, we double-checked our findings using BWA (maximum gap openings = 3, max gap extensions = 100) as a second read mapper. Both aligners yielded comparable results (data not shown).

T7 endonuclease I assay

Genomic DNA was PCR amplified using primers flanking the predicted CRISPR cleavage site (e3: Exon 3_fw: 5′-AGAAGTG CATGGCTGGTGAG-3′; Exon 3_rev: 5′-GCAGTCAGAGGACCAGGTCC-3′; e5.1&e5.2: Exon 5_fw: 5′-CTGAGGTGTAGACGCCAACT-3′; Exon 5_rev: 5′-ACCCCAGTTGCAAACCAGAC-3′). After PCR purification using the Qiagen PCR Purification kit according to the

manufacturer's instruction, DNA was denatured and reannealed in 1× NEB2 buffer (NEB, M0302L) using a thermomixer. The reannealed DNA was digested with 5 U T7 endonuclease I (NEB, M0302L) for 20 min at 37 °C and separated on a 2% agarose gel.

qPCR and RTqPCR

100 ng genomic DNA was used as template for qPCR. The presence of *TP53* deletions induced by CRISPR-Cas9 nucleases was quantified in a qPCR reaction on a LightCycler 480 (Roche) with ABsolute QPCR SYBR Green Mix (Thermo Scientific). Primers (Δp53_for 5′-ATAGGGTGC ACATTTAGGAA-3′; Δp53_ rev 5′-GGCTAGGCTAAGCTATGATGTTC-3′) were used at a final concentration of 300 nM. Amplification protocol: initial activation of the Hot Start Taq Polymerase for 10 min at 95 °C, followed by 40 cycles of 15 s at 95 °C and 60 s at 60 °C.

Gene expression analysis was performed as previously described51. Total RNA was isolated with the RNeasy Mini Kit (Qiagen) and cDNA synthesis performed with the SuperScript VILO cDNA synthesis kit (Life Technologies) following manufacturer's instructions. Gene expression was quantified on a LightCycler 480 (Roche) using the ABsolute QPCR SYBR Green Mix (Thermo Scientific). Data were evaluated by the ΔΔCt method. GAPDH was measured as a housekeeping gene for normalization.

Western blotting

Cells were lysed in NP-40 Lysis Buffer (50 mM Tris-HCl, 150 mM NaCl, 5 mM EDTA, 2% NP-40, pH 8.0) supplemented with protease inhibitor (complete ULTRA tablets EASYpack, Roche) and phosphatase inhibitor (PhosSTOP, Roche). Protein yield was determined by Bradford assay (Bio-Rad). Total protein (5–30 μg) was separated on NuPAGE SDS Gels (Life Technologies) and tank-blotted to PVDF or nitrocellulose membranes. Following blocking in Tris-buffered saline with Tween 20 (TBST; 5 mM Tris, 15 mM NaCl, 0.1% Tween 20, pH 7.5) with 5% nonfat dry milk or 5% bovine serum albumin for 2 h, membranes were incubated with primary antibodies diluted in TBST/5% nonfat dry milk or TBST/5% bovine serum albumin and incubated overnight at 4 °C. Antibodies: anti-p53 (Santa Cruz, DO-1, 1:10,000); anti-p53-phosphoSer15 (Cell Signaling, 1:1,000); anti-H2A.X-phosphoSer139 (Abcam, 1:500); anti-p21 (Santa Cruz, C-19, sc-397, 1:200); anti-FancD2 (Santa Cruz, Fl17, sc-20022, 1:500); anti-FancA (Bethyl Laboratories, 1:2,000); anti-FancL (Santa Cruz, H-197, sc-66887, 1:200); anti-Rad18 (Abcam, 1:500); anti-mTOR (Cell Signaling, 7C10, 1:1,000); anti-p70S6K (Santa Cruz, H-9, sc-8418 1:1,000); anti-p70S6K-phospho-Thr389 (Cell Signaling, 1082, 1:10,00); anti-Akt (Cell Signaling, 1:1,000); anti-Akt-phospho-Ser473 (Cell Signaling, 1:1,000); anti-4EBP1-phospho-Thr36/47 (Cell Signaling, 1:1,000); anti-β-actin (Abcam, AC-15, 1:5,000). Proteins were detected with secondary antibody (anti-mouse IgG-HRP, anti-rabbit IgG-HRP from GE Healthcare, 1:3,000) and ECL kit (SuperSignal West Dura Chemiluminescent Substrate, Thermo Scientific). Uncropped versions of all western blots are provided in Supplementary Figures 18-21.

Immunofluorescence

For immunofluorescence staining, cells were seeded with 13,000 (HCT116) or 10,000 (H460) cells per well on a μCLEAR plate (96-well, Greiner bio-one) and treated with 1 μM RITA for 16 h or with 16 μM CDDP for 2 h. Cells were fixed for 15 min at −20 °C using ice-cold methanol/acetone (1:1) and permeabilized with PBS/0.1% NP-40 2 × 5 min at RT. After 45 min of blocking with PBS/0.1% NP-40/5% FCS, the cells were incubated with anti-H2A.X-phospho-Ser139 (1:1,500, Millipore no. 05-636) at 37 °C for 45 min. The samples were then incubated with 200 nM DAPI (Molecular Probes, D-21490) and anti-mouse Alexa 647 (1:400, Molecular Probes, A21236) for 45 min at RT. The fluorescence was then measured on the BD Pathway Bioimager and analyzed with BD AttoVision software.

Statistical analysis

All experimental results are presented as the mean of at least three independent experiments ± s.d., unless otherwise stated. Statistical tests were performed as described in the figure captions. *P* values were corrected for multiple comparisons as reported in the figure captions and were calculated using GraphPad Prism 6 (GraphPad Software, San Diego, CA, USA).

Supplementary Material

Refer to Web version on PubMed Central for supplementary material.

Acknowledgments

We thank B. Vogelstein (John Hopkins University) for providing HCT116 $p53^{-/-}$ cells and A. Filmer for excellent technical assistance with next-generation sequencing. The authors are grateful to the members of the Stiewe laboratory for fruitful discussions and support of the project. This research was supported by Deutsche Forschungsgemeinschaft grants WA 2725/1-1 (M.W.), TRR81 (T.S.), STI 182/3-2 (T.S.) and STI 182/7-1 (T.S.); European Research Council grant P73CANCER 260431 (T.S.); Deutsche Krebshilfe grant 111250 (T.S.); Deutsche José Carreras Leukämie-Stiftung grant (T.S.), Von-Behring-Röntgen-Stiftung grant (T.S.), Rhön Klinikum AG grant (T.S.) and LOEWE Universities of Giessen and Marburg Lung Center grant (T.S.).

References

1. Pant V, Lozano G. Limiting the power of p53 through the ubiquitin proteasome pathway. Genes Dev. 2014; 28:1739–1751. [PubMed: 25128494]
2. Ventura A, et al. Restoration of p53 function leads to tumour regression *in vivo*. Nature. 2007; 445:661–665. [PubMed: 17251932]
3. Martins CP, Brown-Swigart L, Evan GI. Modeling the therapeutic efficacy of p53 restoration in tumors. Cell. 2006; 127:1323–1334. [PubMed: 17182091]
4. Xue W, et al. Senescence and tumour clearance is triggered by p53 restoration in murine liver carcinomas. Nature. 2007; 445:656–660. [PubMed: 17251933]
5. Feldser DM, et al. Stage-specific sensitivity to p53 restoration during lung cancer progression. Nature. 2010; 468:572–575. [PubMed: 21107428]
6. Kandoth C, et al. Mutational landscape and significance across 12 major cancer types. Nature. 2013; 502:333–339. [PubMed: 24132290]
7. Cheok CF, Verma CS, Baselga J, Lane DP. Translating p53 into the clinic. Nat Rev Clin Oncol. 2011; 8:25–37. [PubMed: 20975744]
8. Kussie PH, et al. Structure of the MDM2 oncoprotein bound to the p53 tumor suppressor transactivation domain. Science. 1996; 274:948–953. [PubMed: 8875929]
9. Vassilev LT, et al. *In vivo* activation of the p53 pathway by small-molecule antagonists of MDM2. Science. 2004; 303:844–848. [PubMed: 14704432]

10. Khoo KH, Verma CS, Lane DP. Drugging the p53 pathway: understanding the route to clinical efficacy. Nat Rev Drug Discov. 2014; 13:217–236. [PubMed: 24577402]
11. Michaelis M, et al. Adaptation of cancer cells from different entities to the MDM2 inhibitor nutlin-3 results in the emergence of p53-mutated multi-drug-resistant cancer cells. Cell Death Dis. 2011; 2:e243. [PubMed: 22170099]
12. Garnett MJ, et al. Systematic identification of genomic markers of drug sensitivity in cancer cells. Nature. 2012; 483:570–575. [PubMed: 22460902]
13. Lau LMS, Nugent JK, Zhao X, Irwin MS. HDM2 antagonist Nutlin-3 disrupts p73–HDM2 binding and enhances p73 function. Oncogene. 2008; 27:997–1003. [PubMed: 17700533]
14. Michaelis M, et al. Reversal of P-glycoprotein–mediated multidrug resistance by the murine double minute 2 antagonist nutlin-3. Cancer Res. 2009; 69:416–421. [PubMed: 19147553]
15. Nieves-Neira W, et al. DNA protein cross-links produced by NSC 652287, a novel thiophene derivative active against human renal cancer cells. Mol Pharmacol. 1999; 56:478–484. [PubMed: 10462535]
16. Issaeva N, et al. Small molecule RITA binds to p53, blocks p53–HDM-2 interaction and activates p53 function in tumors. Nat Med. 2004; 10:1321–1328. [PubMed: 15558054]
17. Bunz F, et al. Requirement for p53 and p21 to sustain G2 arrest after DNA damage. Science. 1998; 282:1497–1501. [PubMed: 9822382]
18. Tovar C, et al. Small-molecule MDM2 antagonists reveal aberrant p53 signaling in cancer: implications for therapy. Proc Natl Acad Sci USA. 2006; 103:1888–1893. [PubMed: 16443686]
19. Enge M, et al. MDM2-dependent downregulation of p21 and hnRNP K provides a switch between apoptosis and growth arrest induced by pharmacologically activated p53. Cancer Cell. 2009; 15:171–183. [PubMed: 19249676]
20. Hedström E, Eriksson S, Zawacka-Pankau J, Arnér ESJ, Selivanova G. p53-dependent inhibition of TrxR1 contributes to the tumor-specific induction of apoptosis by RITA. Cell Cycle. 2009; 8:3584–3591. [PubMed: 19838062]
21. Grinkevich VV, et al. Ablation of key oncogenic pathways by RITA-reactivated p53 is required for efficient apoptosis. Cancer Cell. 2009; 15:441–453. [PubMed: 19411072]
22. Weilbacher A, Gutekunst M, Oren M, Aulitzky WE, van der Kuip H. RITA can induce cell death in p53-defective cells independently of p53 function via activation of JNK/SAPK and p38. Cell Death Dis. 2014; 5:e1318. [PubMed: 25010984]
23. Zhao CY, Grinkevich VV, Nikulenkov F, Bao W, Selivanova G. Rescue of the apoptotic-inducing function of mutant p53 by small molecule RITA. Cell Cycle. 2010; 9:1847–1855. [PubMed: 20436301]
24. Burmakin M, Shi Y, Hedström E, Kogner P, Selivanova G. Dual targeting of wild-type and mutant p53 by small molecule RITA results in the inhibition of N-Myc and key survival oncogenes and kills neuroblastoma cells *in vivo* and *in vitro*. Clin Cancer Res. 2013; 19:5092–5103. [PubMed: 23864164]
25. Wei X, et al. A simple statistical test to infer the causality of target/phenotype correlation from small molecule phenotypic screens. Bioinformatics. 2012; 28:301–305. [PubMed: 22155864]
26. Smurnyy Y, et al. DNA sequencing and CRISPR-Cas9 gene editing for target validation in mammalian cells. Nat Chem Biol. 2014; 10:623–625. [PubMed: 24929529]
27. Hsu PD, Lander ES, Zhang F. Development and applications of CRISPR-Cas9 for genome engineering. Cell. 2014; 157:1262–1278. [PubMed: 24906146]
28. Kasap C, Elemento O, Kapoor TM. DrugTargetSeqR: a genomics- and CRISPR-Cas9–based method to analyze drug targets. Nat Chem Biol. 2014; 10:626–628. [PubMed: 24929528]
29. Charles JP, et al. Monitoring the dynamics of clonal tumour evolution *in vivo* using secreted luciferases. Nat Commun. 2014; 5:3981. [PubMed: 24889111]
30. de Lange J, Verlaan-de Vries M, Teunisse AFAS, Jochemsen AG. Chk2 mediates RITA-induced apoptosis. Cell Death Differ. 2012; 19:980–989. [PubMed: 22158418]
31. Niedernhofer LJ, et al. The structure-specific endonuclease Ercc1-Xpf is required to resolve DNA interstrand cross-link–induced double-strand breaks. Mol Cell Biol. 2004; 24:5776–5787. [PubMed: 15199134]

32. Kelland L. The resurgence of platinum-based cancer chemotherapy. Nat Rev Cancer. 2007; 7:573–584. [PubMed: 17625587]
33. Kim H, D'Andrea AD. Regulation of DNA cross-link repair by the Fanconi anemia/BRCA pathway. Genes Dev. 2012; 26:1393–1408. [PubMed: 22751496]
34. Kachnic LA, et al. FANCD2 but not FANCA promotes cellular resistance to type II topoisomerase poisons. Cancer Lett. 2011; 305:86–93. [PubMed: 21414716]
35. Song IY, et al. Rad18-mediated translesion synthesis of bulky DNA adducts is coupled to activation of the Fanconi anemia DNA repair pathway. J Biol Chem. 2010; 285:31525–31536. [PubMed: 20675655]
36. Park HK, Wang H, Zhang J, Datta S, Fei P. Convergence of Rad6/Rad18 and Fanconi anemia tumor suppressor pathways upon DNA damage. PLoS ONE. 2010; 5:e13313. [PubMed: 20967207]
37. Williams SA, Longerich S, Sung P, Vaziri C, Kupfer GM. The E3 ubiquitin ligase RAD18 regulates ubiquitylation and chromatin loading of FANCD2 and FANCI. Blood. 2011; 117:5078–5087. [PubMed: 21355096]
38. Zhang J, Zhao D, Wang H, Lin C-J, Fei P. FANCD2 monoubiquitination provides a link between the HHR6 and FA-BRCA pathways. Cell Cycle. 2008; 7:407–413. [PubMed: 18277096]
39. Pickering A, et al. *In vitro* FANCD2 monoubiquitination by HHR6 and hRad18. Cell Cycle. 2013; 12:3448–3449. [PubMed: 24036990]
40. Shen C, et al. Regulation of FANCD2 by the mTOR pathway contributes to the resistance of cancer cells to DNA double-strand breaks. Cancer Res. 2013; 73:3393–3401. [PubMed: 23633493]
41. Guo F, et al. mTOR regulates DNA damage response through NF-κB–mediated FANCD2 pathway in hematopoietic cells. Leukemia. 2013; 27:2040–2046. [PubMed: 23538752]
42. Krajewski M, Ozdowy P, D'Silva L, Rothweiler U, Holak TA. NMR indicates that the small molecule RITA does not block p53–MDM2 binding *in vitro*. Nat Med. 2005; 11:1135–1156. [PubMed: 16270059]
43. Visvader JE, Lindeman GJ. Cancer stem cells in solid tumours: accumulating evidence and unresolved questions. Nat Rev Cancer. 2008; 8:755–768. [PubMed: 18784658]
44. Beck B, Blanpain C. Unravelling cancer stem cell potential. Nat Rev Cancer. 2013; 13:727–738. [PubMed: 24060864]
45. Bertolini G, et al. Highly tumorigenic lung cancer $CD133^{+}$ cells display stem-like features and are spared by cisplatin treatment. Proc Natl Acad Sci USA. 2009; 106:16281–16286. [PubMed: 19805294]
46. Meng X, Wang X, Wang Y. More than 45% of A549 and H446 cells are cancer initiating cells: evidence from cloning and tumorigenic analyses. Oncol Rep. 2009; 21:995–1000. [PubMed: 19287999]
47. Chresta CM, et al. AZD8055 is a potent, selective, and orally bioavailable ATP-competitive mammalian target of rapamycin kinase inhibitor with *in vitro* and *in vivo* antitumor activity. Cancer Res. 2010; 70:288–298. [PubMed: 20028854]
48. Guzmán C, Bagga M, Kaur A, Westermarck J, Abankwa D. ColonyArea: an ImageJ plugin to automatically quantify colony formation in clonogenic assays. PLoS ONE. 2014; 9:e92444. [PubMed: 24647355]
49. Ran FA, et al. Genome engineering using the CRISPR-Cas9 system. Nat Protoc. 2013; 8:2281–2308. [PubMed: 24157548]
50. Shalem O, et al. Genome-scale CRISPR-Cas9 knockout screening in human cells. Science. 2014; 343:84–87. [PubMed: 24336571]
51. Schlereth K, et al. DNA binding cooperativity of p53 modulates the decision between cell-cycle arrest and apoptosis. Mol Cell. 2010; 38:356–368. [PubMed: 20471942]

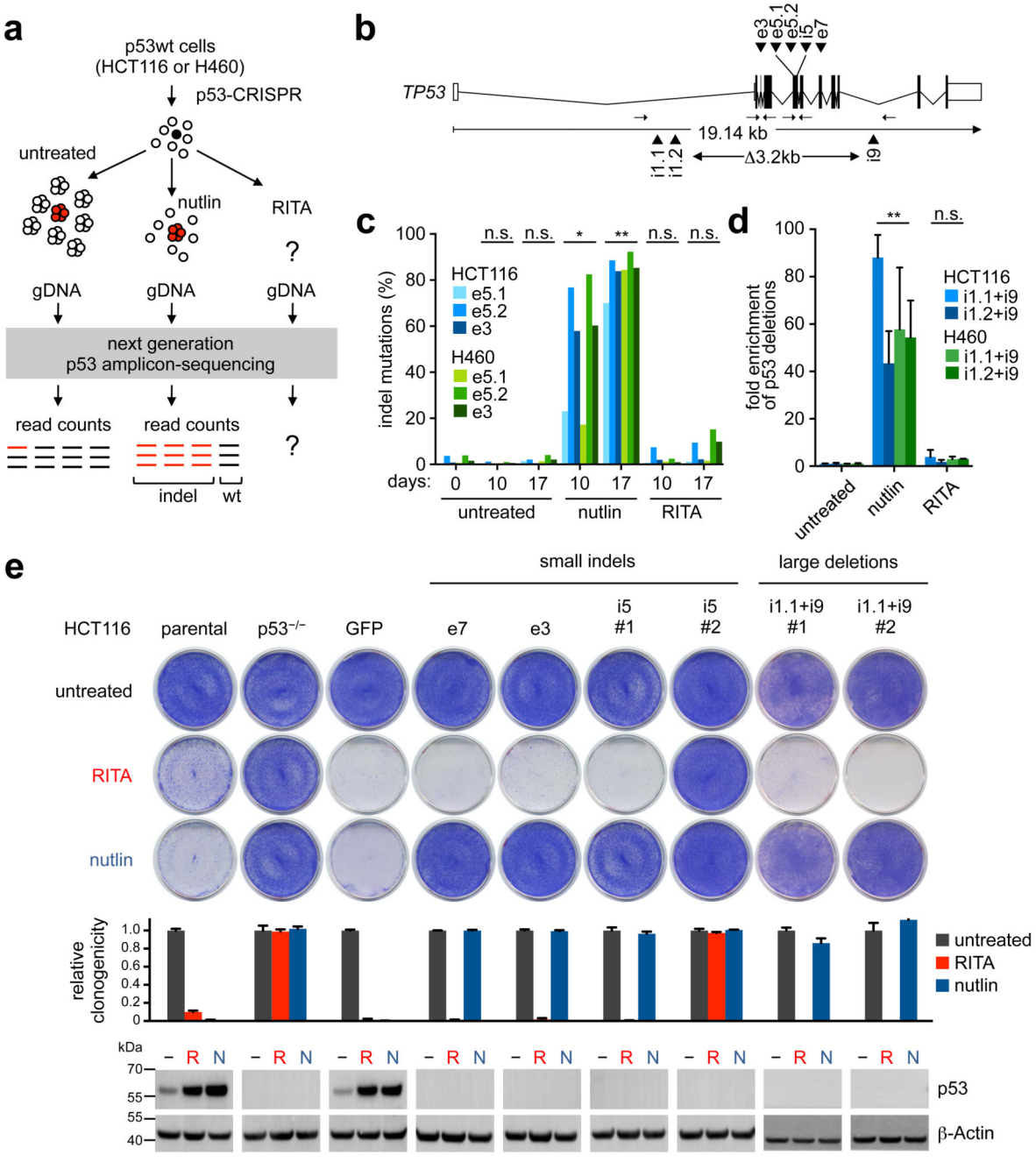

Figure 1. p53-deficient cells are resistant to nutlin but not RITA.

(**a**) Schematic outline of CRISPR-Cas9–based p53 enrichment assay. WT, wild type. (**b**) Schematic representation of the *TP53* gene locus. Cleavage sites (black triangles) of CRISPR-Cas9 nucleases and primers (arrows) used for PCR analysis are indicated. (**c**) Enrichment of cells with *TP53* indel mutations. Shown are percentages of mutated sequencing reads in cells treated with 7 μM nutlin or 1 μM RITA for the indicated time points. Enrichment versus untreated cells at day 0 was tested for significance using the nonparametric Friedman′s test and corrected for multiple comparisons using Dunn′s test

Europe PMC Funders Author Manuscripts

(*$P < 0.05$; **$P < 0.01$; NS, not significant). (**d**) Enrichment of cells with deletion of exons 2–9 in *TP53*. Cells cotransfected with a nuclease pair were treated as in **c** for 10 d and analyzed by qPCR for deletion of exons 2–9. Shown is the fold enrichment in treated versus untreated cells (mean ± s.d., $n = 3$). Enrichment versus untreated cells was tested for significance by nonparametric Friedman′s test corrected for multiple comparisons by Dunn′s test (**$P < 0.01$; NS, not significant). (**e**) Colony formation of HCT116 parental and HCT116 $p53^{-/-}$ (ref. 17) cells under the indicated treatments compared to CRISPR-Cas9-generated single cell clones with small indels or large deletions in *TP53*. 'GFP' represents negative control cells transfected with a GFP-targeted nuclease. Western blots confirm the successful inactivation of p53. Relative clonogenicity is shown as mean ± s.d. ($n = 4$). MW, molecular weight; R, RITA treatment; N, nutlin treatment.

Europe PMC Funders Author Manuscripts

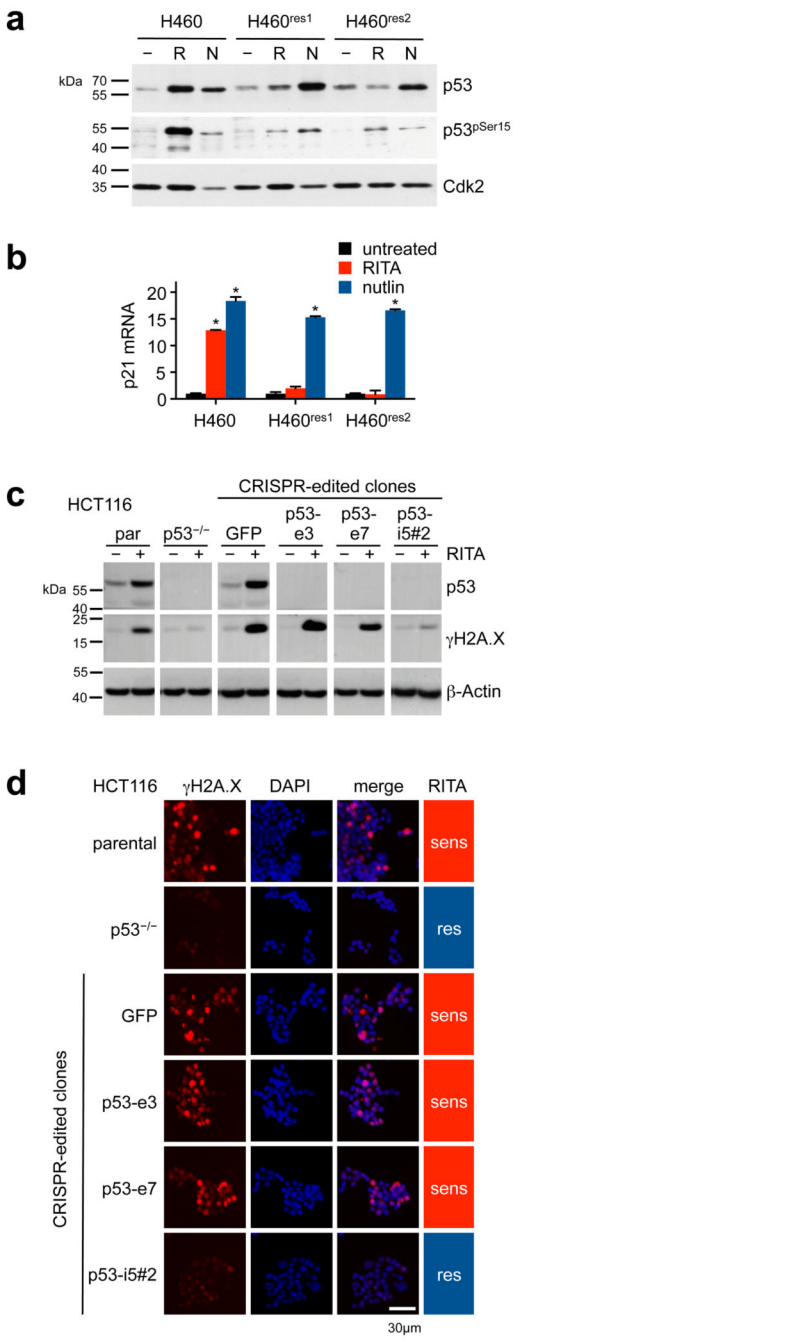

Figure 2. RITA sensitivity correlates with induction of DNA damage.

(**a**,**b**) Expression of p53 protein, p53-Ser15 phosphorylation and p21 mRNA of parental H460 cells and two RITA-resistant H460 cell pools treated as indicated for 24 h (R, 1 μM RITA; N, 10 μM nutlin). p21 expression is shown normalized to GAPDH expression and relative to untreated cells (mean ± s.d. $n = 3$; *, $P < 0.0001$, by two-way analysis of variance and Sidak′s multiple comparisons test) by western blotting (**a**) and RTqPCR(**b**). MW, molecular weight; R, RITA treatment; N, nutlin treatment. (**c**,**d**) Expression of p53 and γH2A.X in parental and HCT116 derivate clones after a 16 h treatment with 1 μM RITA, as

shown by western blotting (**c**) and immunofluorescence (**d**). Color bars indicate RITA sensitivity, as in Figure 1e.

Europe PMC Funders Author Manuscripts

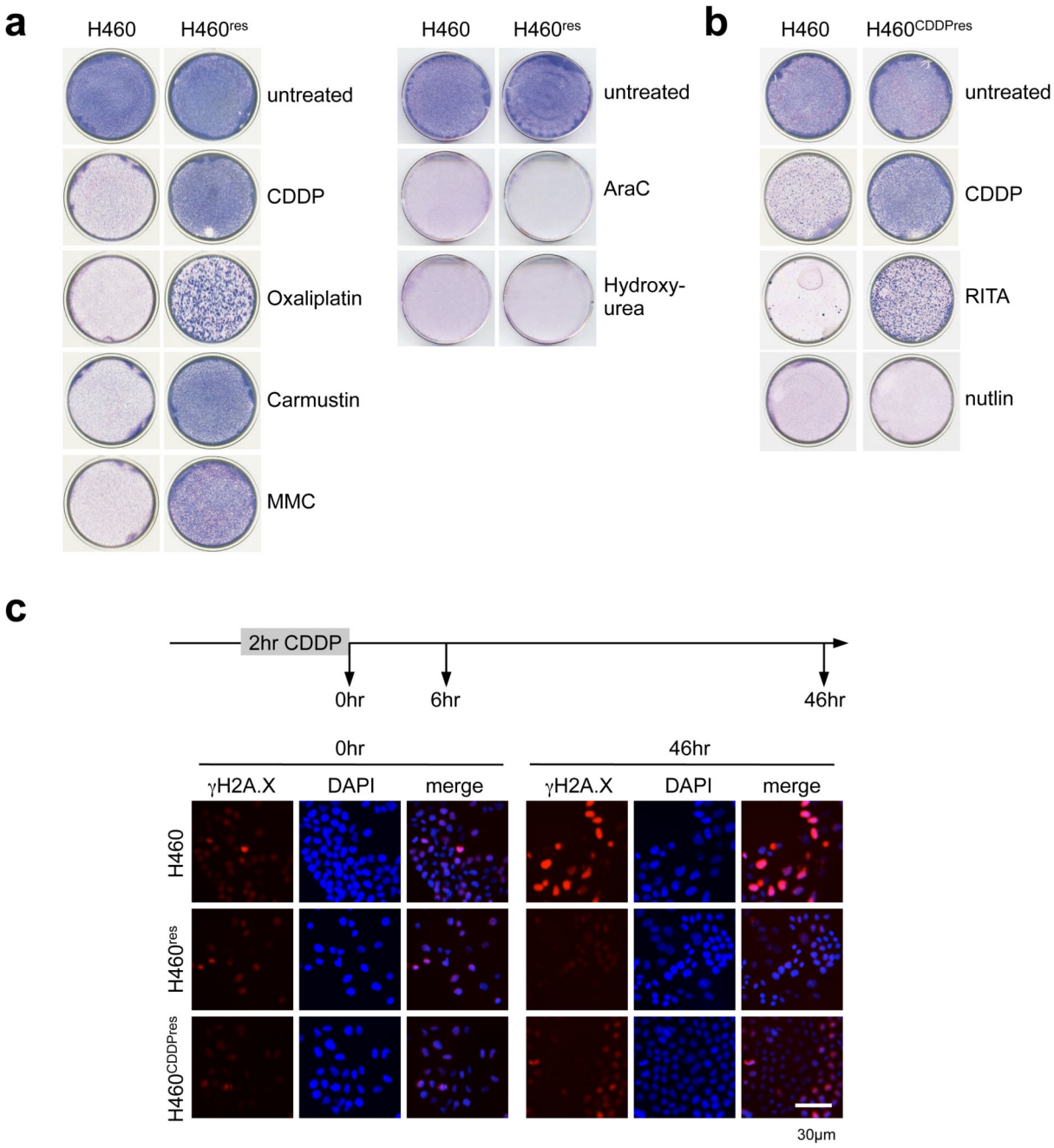

Figure 3. RITA resistant cells are cross-resistant to cisplatin.

(**a**) Colony formation of parental and RITA-resistant H460 cells 7 d following a 3-d treatment with 3 μM CDDP, 8 μg ml^{-1} oxaliplatin, 50 μg ml^{-1} carmustin and 0.05 μg ml^{-1} mitomycin C (MMC) or treated continuously with 0.5 μg ml^{-1} cytarabin (AraC) and 0.5 mM hydroxyurea. (**b**) Colony formation of parental and CDDP-resistant H460 cells continuously treated with 3 μM CDDP, 1 μM RITA and 10 μM nutlin. (**c**) Increased DNA damage repair in RITA- and CDDP-resistant H460 cells. Immunofluorescence analysis of γH2A.X at indicated time points following a 2-h treatment with 16 μM CDDP is shown.

Europe PMC Funders Author Manuscripts

Europe PMC Funders Author Manuscripts

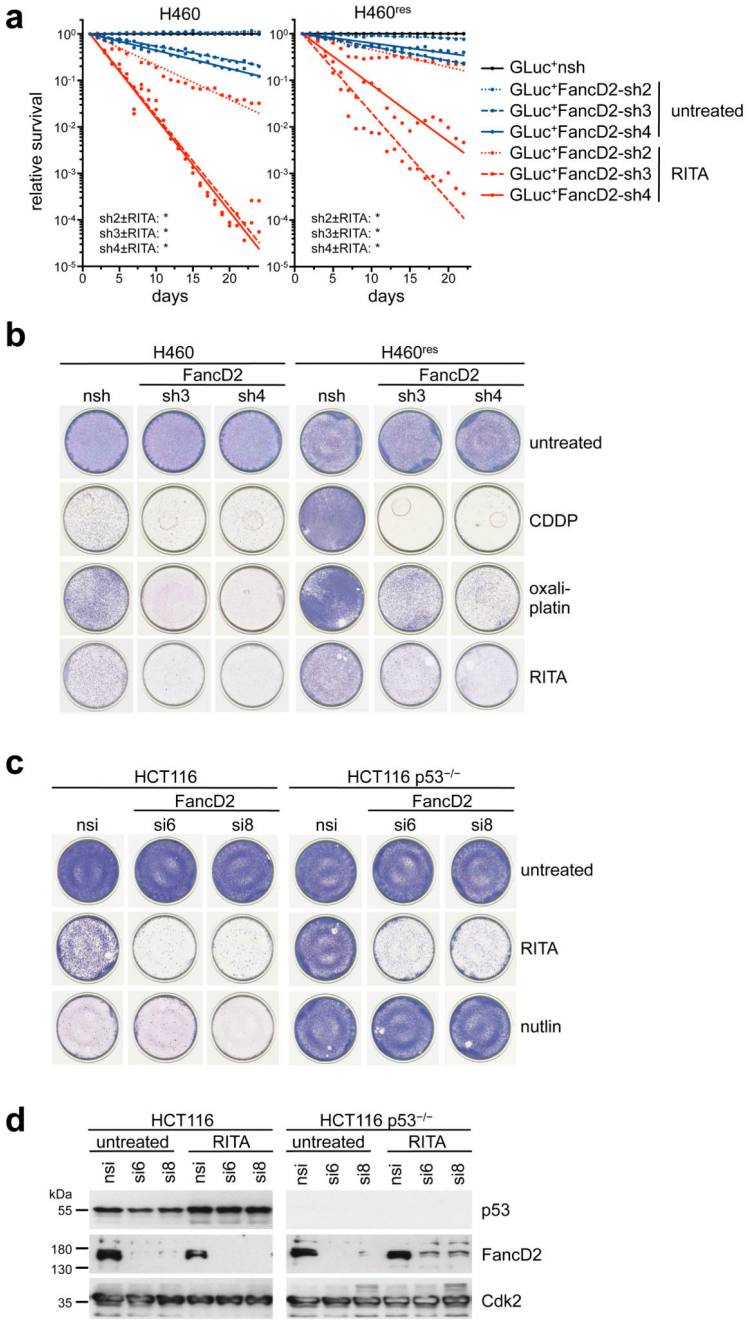

Figure 4. RITA resistance is mediated by FancD2.

(**a**) Parental and RITA-resistant H460 cells transduced with lentiviral vectors expressing secreted luciferases (GLuc or CLuc) coupled to shRNA targeting FancD2. FancD2 knockdown sensitizes parental (left) and RITA-resistant (right) H460 cells to RITA in a competitive co-culture setting. Shown is the relative mean survival of $GLuc^+$ cells expressing the indicated shRNAs in 1:1 cocultures with $CLuc^+$ NSH cells assayed in triplicate ($n = 3$) in the absence (blue) or presence (red) of RITA (parental: 0.125 μM, resistant: 2 μM). $*P < 0.0001$; statistical significance between treated and untreated cell

mixtures was assessed by two-way analysis of variance with Tukey's multiple comparisons test. (**b**) Colony formation of parental and RITA-resistant H460 cells transduced with the indicated shRNAs treated continuously with 1 μM RITA or for 3 d with 8 μg ml^{-1} oxaliplatin and 3 μM CDDP. (**c**,**d**) FancD2 knockdown sensitizes parental HCT116 and HCT116 *p53*$^{-/-}$ cells17 to RITA but not nutlin, as shown by a colony formation assay (**c**) and western blotting (**d**). MW, molecular weight; NSH, non-targeting negative control shRNA; NSI, non-targeting negative control siRNA; si6 and si8, FancD2-targeting siRNAs.

Europe PMC Funders Author Manuscripts

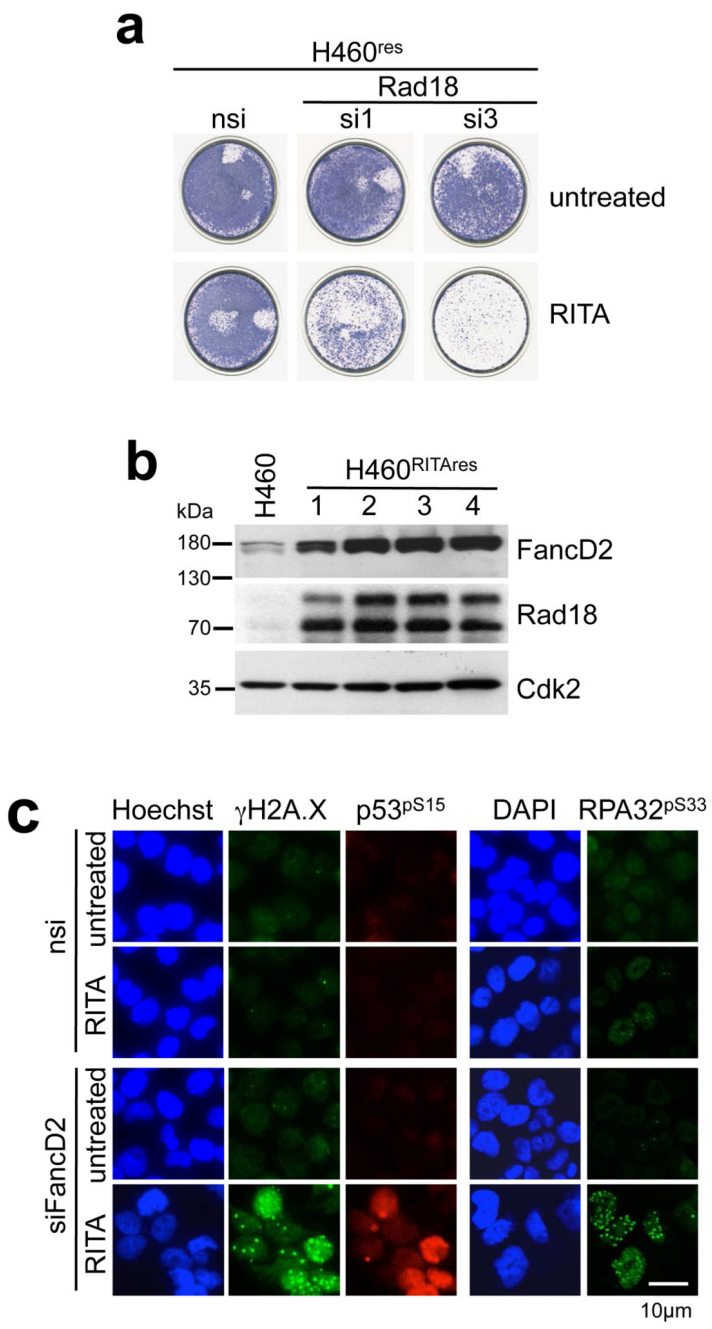

Figure 5. RAD18 depletion sensitizes to RITA.

(**a**) Colony formation of RITA-resistant H460 cells treated with 2 μM RITA following knockdown of Rad18. NSI, non-targeting negative control siRNA; si1 and si3, Rad18-targeting siRNAs. (**b**) Western blotting reveals high-level expression of FancD2 and Rad18 in multiple different RITA-resistant H460 clones compared to parental H460 cells. MW, molecular weight. (**c**) Immunofluorescence analysis indicates induction of DNA damage markers γH2A.X and RPA32 phosphorylated at Ser33 (RPA32^{pS33}) in FancD2-depleted H460 cells following 3-d treatment with 2 μM RITA.

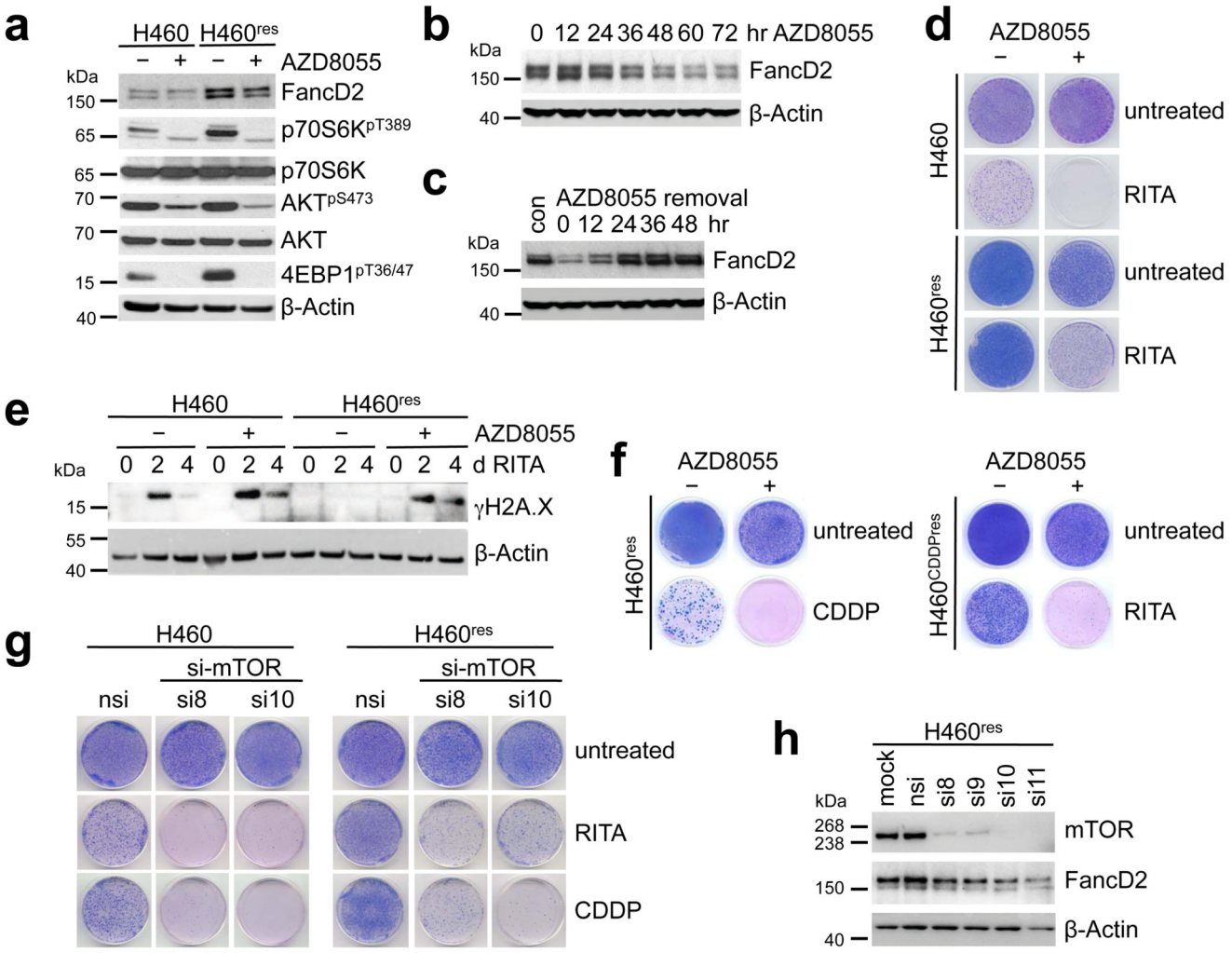

Figure 6. RITA resistance is overcome with mTOR inhibitors.

(**a**) Elevated mTOR signaling in RITA-resistant H460 cells. Western blot of parental H460 and RITA-resistant H460^{res} cells in the presence and absence mTOR kinase inhibitor AZD8055, respectively. MW, molecular weight. (**b**) mTOR inhibition results in progressive downregulation of FancD2 in RITA-resistant H460^{res} cells treated with AZD8055 for the indicated time points. (**c**) FancD2 downregulation by 3-d treatment of RITA-resistant H460^{res} cells with AZD8055 is reversible upon removal of AZD8055 within 24–48 h. (**d**) AZD8055 reduces clonogenic growth of RITA-treated parental and RITA-resistant H460^{res} cells. Cells were grown in the absence or presence of AZD8055 for 3 d, treated with a combination of AZD8055 and RITA for 3 d, and finally treated with RITA only for a further 7 d. H460, 1 μM RITA; H460^{res}, 2 μM RITA. (**e**) AZD8055 treatment enhances γH2A.X induction by RITA. (**f**) AZD8055 reduces clonogenic growth of RITA-resistant H460^{res} cells treated for 3 d with 3.3 μM CDDP and of CDDP-resistant H460^{CDDP} treated continuously with 1 μM RITA. (**g**,**h**) mTOR knockdown reduces clonogenic growth of parental H460 and RITA-resistant H460^{res} cells treated continuously with 1 μM RITA or for 3 d with 3.3 μM CDDP. Western blotting confirms mTOR knockdown efficiency. In all experiments,

Europe PMC Funders Author Manuscripts

AZD8055 was used at 1 μM for H460 and at 2 μM for $H460^{res}$ and $H460^{CDDPres}$. si8-11, mTOR-targeting siRNAs.

Europe PMC Funders Author Manuscripts